An Arm Suspension Mechanism for an Underactuated Single Legged Hopping Robot.

Christopher Schmidt-Wetekam, Thomas Bewley

Abstract—The geometry, kinematics, and mechanical development of a symmetric and adjustable arm suspension mechanism for an actively stabilized single-legged hopping robot are presented. This mechanism is a key enabling design feature of a recently developed two-armed reaction wheel stabilized monopod, that is capable of conventional wheeled roving, continuous hopping, and self-uprighting. The mechanism is shown to behave essentially as a digressive-rate torsional spring placed between the two arms, in series with a weaker progressive-rate torsional spring tied to the leg/central body. This makes it well-suited to recovering substantial energy from hopping motion, whilst presenting negligible resistance to antisymmetric motions used to maintain side-to-side stability. Furthermore, by storing energy purely in tension, the problem of buckling encountered with compression springs is avoided, and, the effective torsional spring constant may be varied by adjusting the spring pretension. Finally, the mechanism is self-latching near maximum deflection, allowing the vehicle to fold into a compact roving configuration, and enabling "running jumps" via the release of this gradually accumulated spring energy.

I. INTRODUCTION

Robots vastly outperform their human counterparts in repetitive, precise tasks such as manufacturing, yet most lack the mobility to compete in even simple tasks such as climbing stairs. This difficulty arises chiefly from the requirements of high power-density, and complex, real-time path-planning for controlling a humanoid robot with a high number of degrees of freedom. Therefore, mechanically simple robots that operate in unstable modes in order to enhance agility have gained research interest. A classic example is the monopedal hopping robot, or "self-balancing" pogo-stick, the most well-known of which was originally demonstrated by Marc Raibert at MIT in the 1980's [1]. Raibert's hopper was hydraulically actuated using offboard power, and was able to control its orientation and forward speed by a combination of foot placement and torque applied between the leg and main body of the robot. Other notable monopedal designs incorporating on-board battery power have been created since [2], [3], however, none of these designs are capable of self-uprighting if they fall over.

In the spring of 2003, a natural evolution of this design was proposed: a reaction wheel stabilized monopod (fig. 1). The robot's two main drive wheels roll efficiently over smooth terrain, yet serve also to upright the robot, and, in coordination with an orthogonal set of wheels, stabilize the robot during flight, by exchanging angular momentum between the leg

The authors are affiliated with the Coordinated Robotics Lab, UC San Diego, La Jolla, CA 92093-0411 USA; e-mail: cmschmid@ucsd.edu, bewley@ucsd.edu
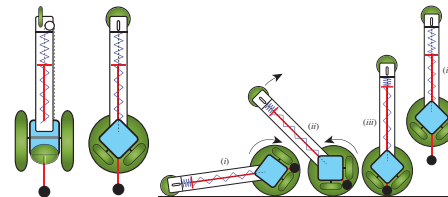
Fig. 1. Cartoons illustrating the multimodal dynamic robot concept. As seen at the right, the proposed vehicle can roll around in a horizontal roving mode (i), transition (ii) to a vertical roving mode (iii), and, when necessary, hop over obstacles (iv).

Fig. 2. Three-wheeled hopping robot, "iHop v.2" prototype. During hopping maneuvers, a reaction wheel centrally-housed within the main body stabilizes about the roll axis, and the two drive wheels stabilize about the pitch axis. A dual four bar hopping mechanism creates linear leg motion with a torque/force relationship favorable for DC motor actuation, and stores hopping energy during roving by latching into a fully-tensioned state.

and the wheels. Several working prototypes based upon this concept have been developed; most notably, "iHop v.2" (fig 2) which incorporated a dual four-bar hopping mechanism, and an "H-Pattern" reaction wheel array (RWA), consisting of a large central reaction wheel mounted orthogonally between two drive wheels [4].

II. MOTIVATION: CHALLENGES WITH REACTION WHEEL STABILIZATION

A. Background

The term "reaction wheel" refers to a driven flywheel that is used to regulate the attitude of any attached bodies about the wheel's axis of rotation, as depicted in fig. 3. They are commonly installed in an x,y,z array on small satellites, however have also been used to stabilize terrestrial platforms [5],[6].

The optimal reaction wheel design for inverted pendulum stabilization is not necessarily the one with the largest angular
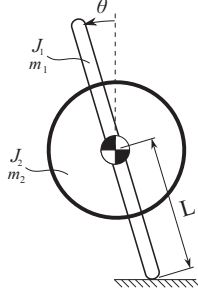
Fig. 3. Single-axis reaction wheel stabilized inverted pendulum. A motorized flywheel (J_2,m_2) stabilizes a rigid body (J_1,m_1) via torque applied by a DC motor with torque constant, k_t, gear reduction, γ, resistance, R, and voltage input, u.
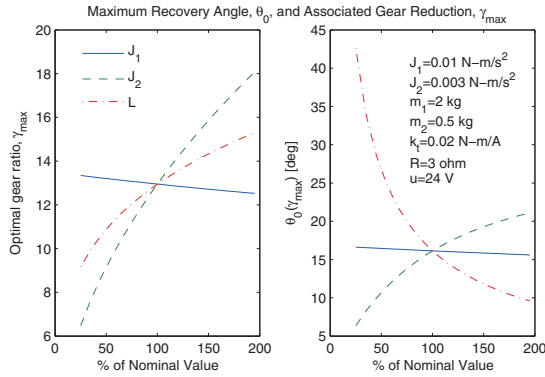

Fig. 4. Maximum recovery angle and associated gear reduction from zero-velocity initial conditions for a single-axis inverted pendulum stabilized via a DC motor driven reaction wheel (fig. 3). Three main parameters are varied: body rotational inertia, J_1, reaction wheel rotational inertia, J_2, and distance from ground pivot point to center of mass, L. For simplicity, it is assumed in this analysis that the reaction wheel rotational inertia can be varied without affecting the system's center of mass.

momentum capacity, since increasing the rotational inertia and top speed also increases the flywheel size (raised center of mass), and decreases the torque output. Specifically, the flywheel properties and gear ratio that maximize the basin of attraction depend specifically on the peak actuator power input, and the mass properties of the entire vehicle. For the system with the mass properties shown in fig. 4, a high-torque/low-speed flywheel with a large moment of inertia, J_2, maximizes the recovery angle (the angle from which the system is able to recover, starting from zero velocity initial condition). Increased body inertia, J_1 only slightly diminishes the recovery angle, however, also decreases robustness to steady-state estimation errors, by virtue of the fact that large external disturbances will cause smaller changes in orientation, which may be obscured by sensor noise.

B. Reaction Wheel Arrays

The addition of orthogonal reaction wheels, for controlling multiple DOF, reduces overall system performance, and significantly affects the optimal design parameters of each reaction wheel. Configuring the wheels concentrically minimizes the extent to which each reaction wheel is burdened
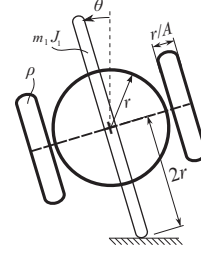

Fig. 5. A 3-wheeled "H-pattern" RWA consisting of a centrally mounted roll axis (θ) wheel of uniform density, ρ, radius, r, and thickness, r/A, surrounded by two orthogonal drive wheels with identical mass properties. The wheels are mounted $2r$ above the foot in order to create consistent ground clearance to the outer wheels for nonzero θ.
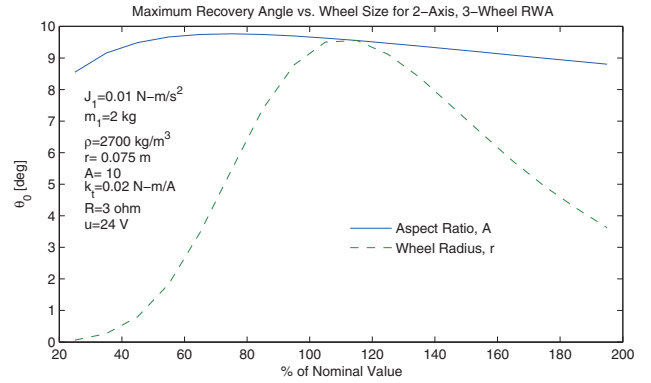

Fig. 6. Maximum roll axis recovery angle for a generic H-pattern RWA (fig. 5), as a function of: wheel radius (dashed), and wheel thickness/aspect ratio (solid). The applied torque, $\tau = \frac{k_t}{R}(u - k_t\omega)$, where ω is the reaction wheel angular velocity, and u is a step voltage input.

by the minor-axis moment of inertia of orthogonal wheels, however is not suitable for a roving operation in which least two parallel drive wheels control both speed and direction.

The H-pattern RWA used in the iHop v.2 prototype (fig. 5) is the simplest fixed configuration suitable for multimodal operation, but is fundamentally limited in terms of performance by the central reaction wheel. Approximating all three reaction wheels as solid, uniform density discs, and assuming that the ground clearance to the wheels is equal to the wheel radius, results in a unique wheel radius for which the maximum recovery angle is achieved (fig. 6). This outcome is rather intuitive in light of the fact that a large center wheel increases and elevates the center of mass, and also increases the minor axis rotational inertia of the orthogonal wheels. Testing on the iHop v.2 prototype confirms the weakness of the roll axis reaction wheel, particularly as bias in the angular estimate develops during hopping maneuvers.

III. ARM SUSPENSION DESIGN FOR UNDERACTUATED STABILIZATION OF HOPPING

A two-armed, two-wheeled vehicle design has been developed in order to overcome the performance limitations of the H-pattern array (fig. 7). This design, consisting of two independently actuated arms with wheels mounted at the
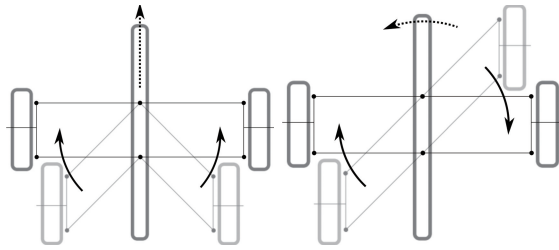
Fig. 7. Independently pivoting reaction wheel configuration. Two main drive wheels mounted at the ends of independently actuated arms produce hopping and/or stabilization motion via a combination of symmetric and antisymmetric rotation. Parallelogram linkages within each arm preserve the relative orientation of the wheels, so as to properly align the wheels for roving, and to minimize coupling of the pitch/roll/yaw axis dynamics.

Fig. 8. The suspension mechanism consists of two symmetric halves that are mounted in separate planes to prevent collisions.

ends, produces hopping motion when the arms are symmetrically actuated, and generates roll-axis reaction torque when the arms are antisymmetrically actuated. This arrangement is degree three underactuated during hopping, as two control inputs (left arm, right arm) simultaneously control the attitude, and x-y position of the central body, as well as the attitude of each arm. This underactuated design reduces the overall robot mass, and enables resources to be shared between the hopping and stabilization functions. The same degree of underactuation has already been successfully demonstrated for a planar monopod [7].

A. Independently Pivoting Reaction Wheel Pair Concept

Several unique design challenges arise in a configuration in which the arms simultaneously produce hopping motion and provide stabilization. Most importantly, the arms must be "antisymmetrically compliant", so as not to stifle stabilizing motions, yet be "symmetrically stiff", in order to passively support the heavy drive wheels and store energy, when deflected, for hopping. While simply placing a torsion spring across the arms would fulfill these requirements, additional design constraints necessitate a more involved solution.

Each arm is actuated by torque applied at one of the outward joints by a high-speed / low-torque motor, therefore, a digressive symmetric stiffness (decreasing with increasing deflection) is desirable in order to provide high support at small deflections, without overwhelming the motors at large deflections. The digressive stiffness emulates a "soft" mechanical stopper when the arms become aligned (180 degrees apart), that efficiently converts angular momentum into linear momentum at takeoff.

In order to store energy for large "running" jumps initiated during forward roving (for instance in order to jump across a chasm), the arms must latch into a fully-tensioned state as they fold into the compact roving mode. A latching action is preferred, as this eliminates the need for added actuators (clutches, ratchets), which are succeptible to jamming under high loads. Furthermore, the latching angle must be less than 90 degrees from horizontal in order to prevent collision between coplanar mechanism links, which also simplifies the
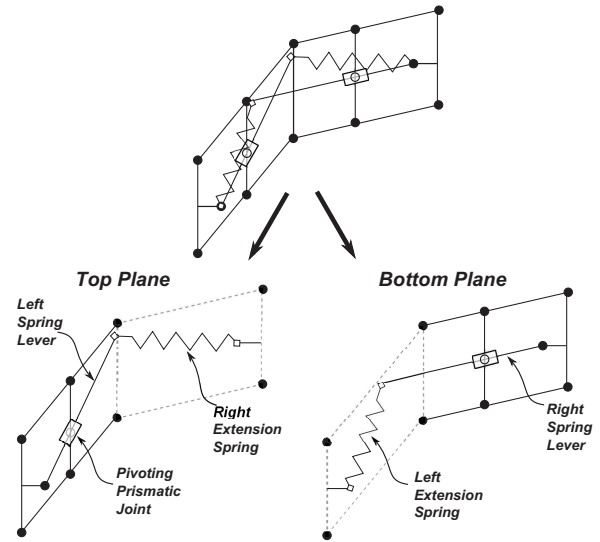
vehicle dynamics by enabling the arm axes of rotation to be collocated.

Lastly, in order to enable "end-over-end" hopping, the spring resistance must be symmetric about the horizontal axis; the ability to adjust the spring stiffness without altering this symmetry is also desired.

B. Arm Suspension Mechanism Layout

The design constraints for this mechanism differ significantly from those encountered for existing legged robots employing leg mechanisms [8]. The parallelogram linkage comprising the "frame" of each arm is based upon suspension designs used in high-performance vehicles, which serves to maintain parallel alignment of the reaction wheels with respect to each other, and to the rest of the robot. This is necessary for efficient wheeled locomotion, as well as to decouple the pitch and roll axis dynamics by ensuring that the effect of the reaction wheel torque on the body is not a function of arm position or velocity.

A parallelogram arm mechanism suspended via two adjustable extension springs has been developed in order to address these design constraints. Each extension spring ties the end of one arm to "spring lever" of the opposite arm. The spring levers slide along prismatic joints that pivot about a central link within the respective parallelogram mechanism (fig. 8).

C. Suspension Mechanism Kinematics

Each arm suspension mechanism plane has one degree of freedom: the left arm frame angle, α_L, for the top plane, and the right arm frame angle, α_R, for the bottom plane, involving the interaction of five interconnected bars (fig. 9).

Defining the origin as the midpoint of the central arm support, the coordinates of first the spring attachment, S_{L1}, are given by
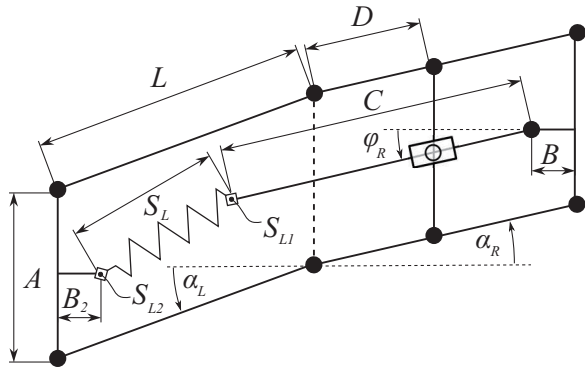
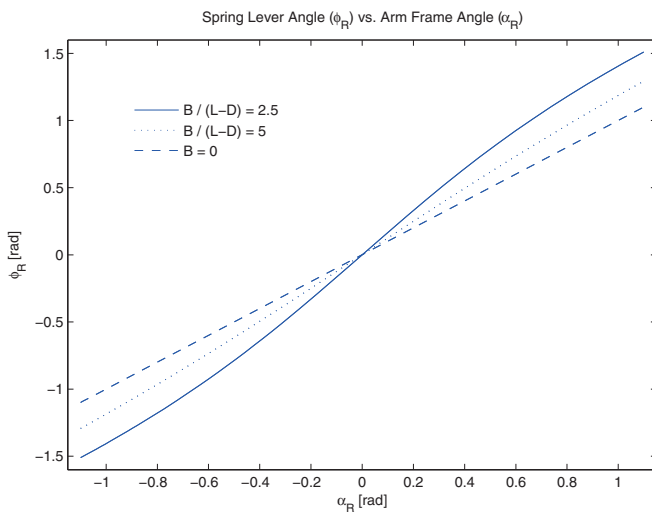Fig. 9. Geometry of bottom linkage plane. The left spring length S_L varies as a function of the left and right arm angles, α_L and α_R.
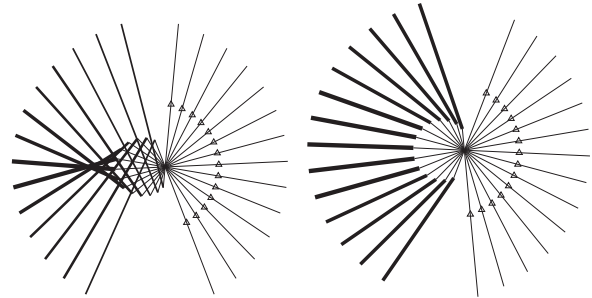

Fig. 11. Lever (solid), fulcrum (triangle), and spring (thick solid) positions throughout the nominal range of symmetric (left) and antisymmetric (right) motion, for bottom linkage plane.

Spring Lever Angle (ϕ_R) vs. Arm Frame Angle (α_R)

B / (L–D) = 2.5
B / (L–D) = 5
B = 0

Fig. 10. The relationship between arm angle, α, and lever angle, ϕ becomes increasingly nonlinear as the spring lever attachment is offset inwards from the arm frame.
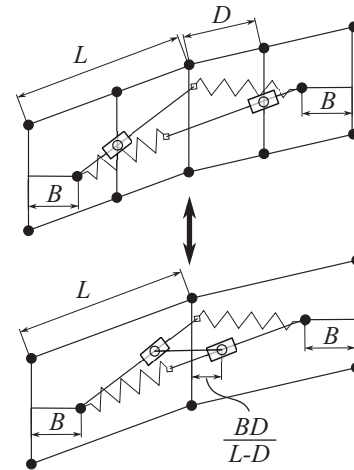

Fig. 12. Two mechanism realizations with equivalent kinematics.

Therefore, a kinematically equivalent mechanism can be constructed by rigidly attaching the spring lever fulcrum to the central leg (fig. 12). As B and D are lengthened, F moves away from the origin, and the spring lever motion becomes less parallel. Recall that strictly parallel motion occurs for $B = 0$, which is in agreement with the fact that F is at the origin for $B = 0$. The latter linkage configuration may be more desirable as it uses four fewer revolute joints, and exerts lighter radial loads on the spring lever support joints, however, it is more challenging to package around other hardware.

D. Suspension Mechanism Spring Action

The left spring vector, $S_L = S_{L2} - S_{L1}$, is given by:

$$S_L = \begin{bmatrix} B + B_2 + C \cos \phi_R - L \left(\cos \alpha_R - \cos \alpha_L \right) \\ C \sin \phi_R - L \left(\sin \alpha_R - \sin \alpha_L \right) \end{bmatrix} \quad (4)$$

The left spring length

$$\| S_L \|^2 = 4 L^2 + 4 B^2 + C^2 - 8 L B \cos \alpha \\ - 4 L C \cos \left(\alpha - \phi_R \right) + 4 B C \cos \phi_R \quad (5)$$

for symmetric rotation ($\alpha_L = -\alpha_R$), and

$$S_{L1} = \begin{bmatrix} L \cos \alpha_R - B - C \cos \phi_R \\ L \sin \alpha_R - C \sin \phi_R \end{bmatrix} \quad (1)$$

where the angle of the "spring lever" (length C), as a function of the respective arm frame angle,

$$\phi_R = -\tan^{-1} \left(\frac{(L - D) \sin \alpha_R}{(L - D) \cos \alpha_R + B} \right) \quad (2)$$

Each spring lever moves parallel to its respective arm frame ($\phi_R = \alpha_R$), when each spring lever attachment is coincident with its respective arm frame (when $B = 0$). As B is increased, the motion of the spring lever becomes increasingly non-parallel relative to its respective arm frame, with a significantly increased sensitivity near horizontal (fig. 10).

Interestingly, the spring lever center of rotation is fixed for both symmetric and antisymmetric rotation (fig. 11), at the position

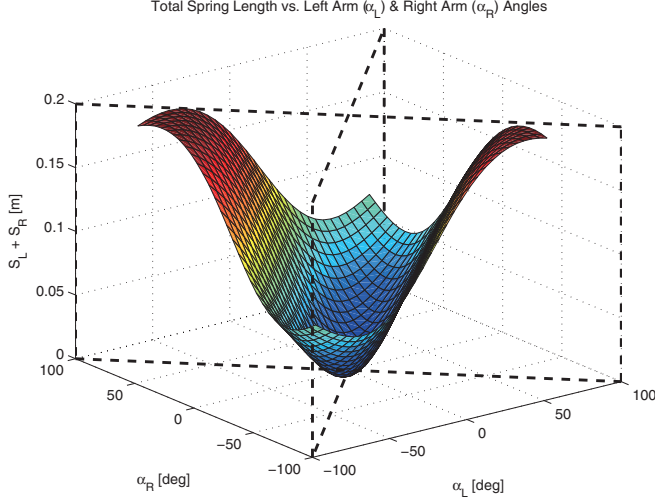$$F = \begin{bmatrix} \frac{BD}{L - D}, 0 \end{bmatrix} \quad (3)$$

Fig. 13. Total spring length as a function of left arm angle (α_L), and right arm angle (α_R). $\frac{B}{L} = \frac{B_2}{L} = 0.125$, $\frac{C}{L} = 1.094$, $\frac{D}{L} = 0.438$

$$\| S_L \|^2 = 4 L^2 \cos \alpha^2 + 4 B^2 + C^2 - 8 LB \cos \alpha$$
$$- 4 LC \cos \phi_R \cos \alpha + 4 BC \cos \phi_R \qquad (6)$$

for antisymmetric rotation ($\alpha_L = \alpha_R$), when $B = B_2$.

Therefore, no spring deflection occurs when $B = 0$ and $C = L$, and the minimum spring length,

$$S_{L0} = 2L - 2B - C \qquad (7)$$

occurs at $\alpha_L = \alpha_R = 0$ (arms 180 degrees apart and orthogonal to leg).

The total spring deflection is symmetric about the axes of symmetric and antisymmetric rotation, with a greater sensitivity to symmetric (hopping) motion (fig. 13) .

As the extension springs are pretensioned, both the symmetric and antisymmetric torsional stiffness increase near zero degrees (figs. 14, 15). The symmetric stiffness is digressive (decreases with increasing deflection), creating a more constant resistive torque that facilitates a large range of motion using a high-speed/low-torque motor. By comparison, the antisymmetric stiffness is much weaker and, for low pretension, is progressive (increases with increasing deflection), as is suitable for accommodating small antisymmetric corrections necessary for active stabilization, while behaving in some sense as a soft limit near the full extent of angular displacement.

E. Suspension Mechanism Latching Properties

The arms automatically latch under maximum tension, since, for symmetric rotation, the resultant spring torque changes sign as the arm angles exceed $\alpha_{max} = +/-65°$ (fig. 14). The latching angle cannot be solved for directly, however, varies between $+/-40°$ to $+/-70°$ from horizontal, and increases primarily as the spring lever, C, is lengthened, (fig. 16).
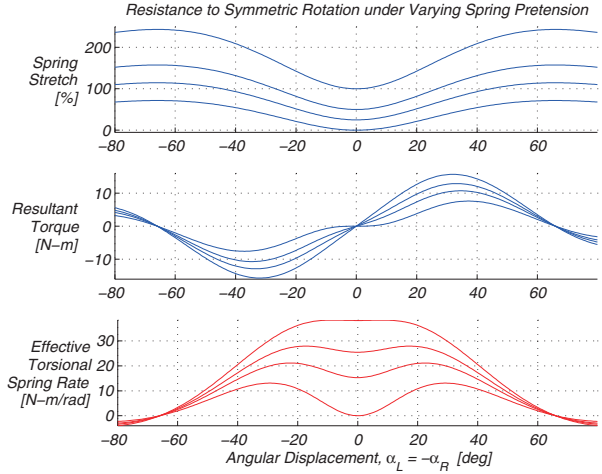

Fig. 14. Total displacement, torsional resistance, and stiffness for purely symmetric (hopping) motion. Self-latching occurs as the torsional resistance crosses zero, at $\alpha = +/-65°$. Added spring pretension significantly stiffens symmetric motion about the rest position.
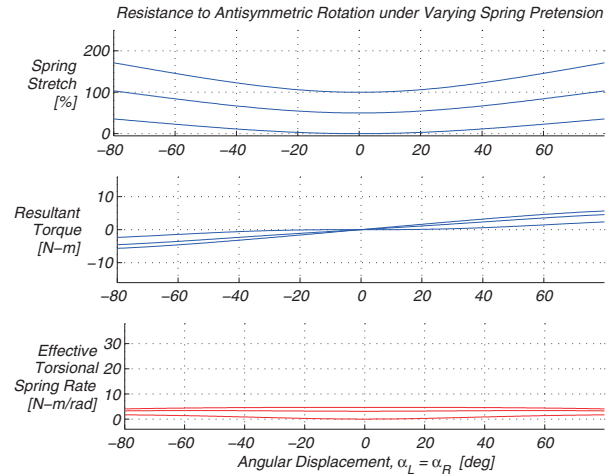

Fig. 15. Total displacement, torsional resistance, and stiffness for purely antisymmetric (balancing) motion. The resistance profile becomes more linear as spring pretension is added, resembling a conventional torsional spring.

IV. WORKING PROTOTYPE

A working prototype employing the linkage design has been fabricated from a combination of 1/16" thick aluminum sheet, and 3/4" square, 1/16" wall aluminum tubing, with 1/4" I.D. ball bearings used in the joints attaching the arms to the central leg, and 1/8" I.D. bronze sleeve bearings are used elsewhere. (fig. 17). Curved arms are used in the physical prototype, in order to permit coplanar placement of members in each half of the mechanism, creating a load path free of any cantilevered supports. Furthermore, in order to avoid linear bearings, the constructed prototype employs a Watts straight-line linkage in place of the prismatic spring lever fulcrum joint. Elastomer spear gun springs are used in the arm suspension, and the entire vehicle weighs 3.5 kg,
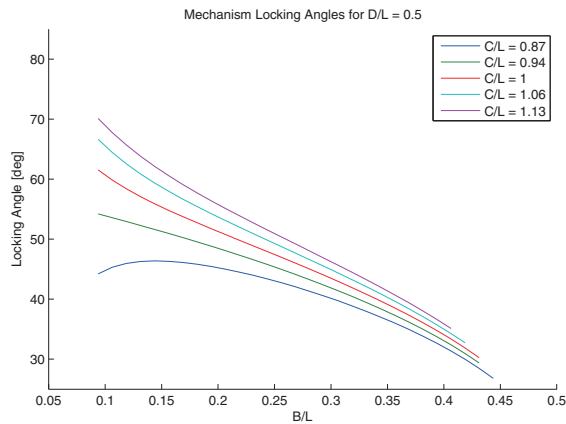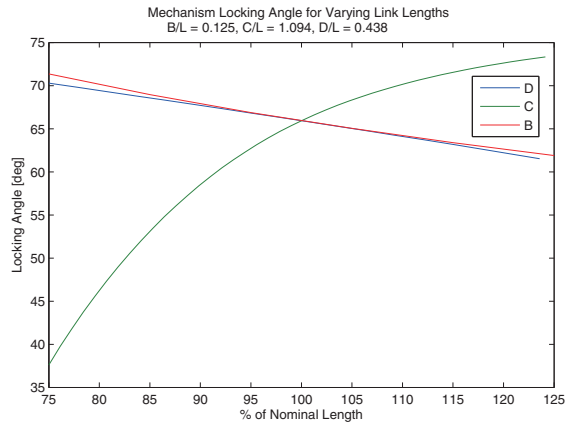
Fig. 16. The arm mechanism latching angle is a function of the linkage lengths B, C, and D. It is most sensitive spring bar length, C, particularly for small B and D.

Fig. 17. "iHop v.3" prototype featuring independently actuated arms suspended via two spring-coupled linkages mirrored about the vertical axis.

the mechanism possesses two unique unstable equilibria, resulting in a latching behavior as the springs reach their maximum tension. Geometric symmetry of the mechanism enables bidirectional arm operation necessary for attempting "end-over-end" hopping and climbing maneuvers. Future work will focus on implementing such advanced maneuvers on the physical prototype, as well as investigating alternative symmetric actuation policies, in order to raise hopping efficiency by decreasing stalled operation, and by adding hopping energy during flight.

including batteries and electronics.

This prototype has already demonstrated the ability to execute feedback-stabilized monopedal locomotion, while maintaining a continuous hopping height of 5 cm under bang-bang control input at 9.6 Volts (35% PWM duty cycle). The hopping performance is less efficient than the previous prototype, due to the significant unsprung mass (0.5 kg) of the rigid central leg, in addition to the rotational inertia of the arms. The details regarding the control design are beyond the scope of this paper, however, videos of the robot are available online.

V. CONCLUSION

An adjustable suspension mechanism suitable for supporting the arms of a multimodal reaction wheel stabilized hopping robot has been successfully demonstrated on a working prototype. The arm suspension mechanism engages two extension springs, and behaves similarly to an adjustable torsional spring, producing large resistance to hopping motion and small resistance to stabilizing motion. As the extension springs are pretensioned, the symmetric stiffness becomes increasingly digressive, which is complementary to hopping motion actuated via DC gearmotor torque. Furthermore,

REFERENCES

[1] M. H. Raibert, H. B. Brown and M. Chepponis, "Experiments in balance with a 3D one-legged hopping machine," Int. J. Robot. Res. 3(2), 75-92 (1984).

[2] H. Rad, P. Gregorio and M. Buehler, "Design, Modeling and Control of a Hopping Robot," Proceedings of IROS, Yokohama, Japan (Jul. 1993) pp. 1778-1785

[3] B. Brown and G. Zeglin, "The Bow Leg Hopping Robot" Proceedings of IEEE International Conference on Robotics and Automation, Leuven, Belgium (May 1998) pp. 781-786

[4] C. Schmidt-Wetekam, D. Zhang, R. Hughes, & T. Bewley (2007) Design, optimization, and control of a new class of reconfigurable hopping rovers. 48th IEEE CDC, 5150 - 5155.

[5] http://www.murataboy.com/en/index.html

[6] Block, D.J., Astrom, K.J., and Spong, M.W., The Reaction Wheel Pendulum, Morgan & Claypool Publishers, 2007.

[7] N. Cherouvim and E. Papadopoulos, "Single actuator control analysis of a planar 3 DOF hopping robot," In: Chapter in Robotics: Science and Systems I (Thrun et al., eds.) (MIT Press, Cambridge, Massachusetts, 2005).

[8] K. V. Papantoniou, "Electromechanical Design for an Electrically Powered, Actively Balanced One Leg Planar Robot," Proceedings of IROS, Workshop on Intelligence for Mechanical Systems, Osaka, Japan (Nov. 1991) pp. 1553- 1560